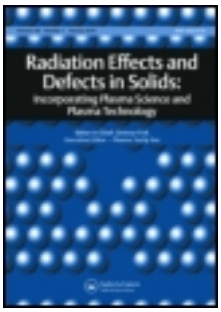

Radiation Effects and Defects in Solids: Incorporating Plasma Science and Plasma Technology

Publication details, including instructions for authors and subscription information:
http://www.tandfonline.com/loi/grad20

Laser irradiation effects on the surface, structural and mechanical properties of Al-Cu alloy 2024

Daniel Yousaf [a], Shazia Bashir [a], Mahreen Akram [a], Umm-i-kalsoom [a] & Nisar Ali [a]

[a] Centre for Advanced Studies in Physics, G. C. University, Lahore, 54000, Pakistan

Published online: 12 Sep 2013.

To cite this article: Daniel Yousaf, Shazia Bashir, Mahreen Akram, Umm-i- kalsoom & Nisar Ali, Radiation Effects and Defects in Solids (2013): Laser irradiation effects on the surface, structural and mechanical properties of Al-Cu alloy 2024, Radiation Effects and Defects in Solids: Incorporating Plasma Science and Plasma Technology, DOI: 10.1080/10420150.2013.834901

To link to this article: http://dx.doi.org/10.1080/10420150.2013.834901

Radiation Effects & Defects in Solids, 2013
http://dx.doi.org/10.1080/10420150.2013.834901

Taylor & Francis
Taylor & Francis Group

Laser irradiation effects on the surface, structural and mechanical properties of Al–Cu alloy 2024

Daniel Yousaf*, Shazia Bashir, Mahreen Akram, Umm-i- kalsoom and Nisar Ali

Centre for Advanced Studies in Physics, G. C. University, Lahore 54000, Pakistan

(*Received 29 April 2013; final version received 8 August 2013*)

Laser irradiation effects on surface, structural and mechanical properties of Al–Cu–Mg alloy (Al–Cu alloy 2024) have been investigated. The specimens were irradiated for various fluences ranging from 3.8 to 5.5 J/cm^2 using an Excimer (KrF) laser (248 nm, 18 ns, 30 Hz) under vacuum environment. The surface and structural modifications of the irradiated targets have been investigated by scanning electron microscope (SEM) and X-ray diffractometer (XRD), respectively. SEM analysis reveals the formation of micro-sized craters along the growth of periodic surface structures (ripples) at their peripheries. The size of the craters initially increases and then decreases by increasing the laser fluence. XRD analysis shows an anomalous trend in the peak intensity and crystallite size of the specimen irradiated for various fluences. A universal tensile testing machine and Vickers microhardness tester were employed in order to investigate the mechanical properties of the irradiated targets. The changes in yield strength, ultimate tensile strength and microhardness were found to be anomalous with increasing laser fluences. The changes in the surface and structural properties of Al–Cu alloy 2024 after laser irradiation have been associated with the changes in mechanical properties.

Keywords: laser fluence; structural modification; mechanical properties; surface morphology

1. Introduction

Laser-material processing is a versatile technique and is highly useful for the surface, structural and mechanical modification of various kinds of materials. Laser-material processing is a subject of considerable interest with its associated vast range of applications in industry, *e.g.* welding, drilling, cutting, surface alloying, cladding, hardening, surface cleaning and phase transformations. Pulsed laser irradiations produce defects and change in the behavior of metals due to the thermal, physical and mechanical effects (*1*, *2*). Dou et al. (*3*) studied surface texturing effects of Al–Cu alloy-2024 using femtosecond and nanosecond pulse laser irradiation and found that surface features ranging from nano to micro-dimensions can be developed through variation in laser fluence intensities. They also observed that ultraviolet laser pulses provide a mechanism for the alteration of surface morphology and texturing without significant damage of the underlying material. Excimer laser irradiation produces kinetically controlled effects in materials which can differ substantially from thermodynamically driven processes.

Al–Cu alloy 2024 is an important engineering material which has high strength to weight ratio, good fatigue resistance; high thermal and electrical conductivity. It is widely used in aircraft,

*Corresponding author. Email: danielyousaf@fccollege.edu.pk

especially wings and fuselage structures. Due to its widespread use in automotive and aerospace industry, it is therefore of fundamental importance and interest to explore the surface, structural and mechanical properties of Al–Cu alloy-2024 after laser irradiation.

In this regard, Hong et al. (*4*) investigated the effects of the laser shock processing on the microstructure, hardness, surface roughness, residual stress, fatigue life and crack growth of Al–Cu alloy 2024. They found that the fatigue life of laser shocked specimen was greater by a factor twice than that of the unshocked specimens. It was also found that the fatigue crack growth at a given stress intensity was reduced by over an order of magnitude. The fatigue behavior improvements are attributed to a combination of increased dislocation density, decreased surface roughness and compressive residual stress induced by laser shock waves. Yang et al. (*5*) discussed the effect of laser shock peening on the fatigue behavior of Al–Cu alloy 2024 under a confined ablation mode using Nd:glass laser and they found that laser shock peening was an effective surface treatment technique for improving the fatigue life of Al–Cu alloy 2024 which was attributed to an introduction of residual compression stress.

In the present work, a pulsed Excimer (KrF) laser of (248 nm, 18 ns, 30 Hz) is employed to irradiate the Al–Cu alloy 2024 for various fluences ranging from 3.8 to 5.5 J/cm^2. The samples were irradiated under vacuum condition. The surface morphological evolution for various laser fluences is investigated by scanning electron microscope (SEM). The novelty of the present work is to correlate surface modification with structural and mechanical properties of irradiated target, explored by X-ray diffractometer (XRD), tensile testing and microhardness techniques. According to our knowledge very little work is reported in which surface, structural and mechanical properties of materials after laser irradiation are discussed. Specifically, for Al–Cu alloy 2024, no work has been reported in which a relationship is established between the surface, structural and mechanical modification of irradiated targets. In these results, it has been reported that up to certain range with increasing laser fluence the generated defects increase and consequently an increase in yield strength (YS) and ultimate tensile strength (UTS) is observed, whereas any further increase in fluence causes a reduction in the defects due to annealing.

2. Experimental work

The Al–Cu alloy 2024 used for this experiment had the following composition of aluminum 93.5%, copper 4.3–4.5%, manganese 0.5–0.6%, and magnesium 1.3–1.5%. Specimens in the form of sheets with thickness of 3 mm, length of 45 mm and width of 6 mm were selected for irradiation. The surface of the samples was polished with silicon carbide (SiC) papers of different progressive grades and then mechanically polished with diamond paste down to rms surface roughness of approximately 10 nm. The surface roughness of the targets was measured by using atomic force microscope (AFM). The rms value of the surface roughness comes out to be 10 nm. The initial rms surface roughness of the target plays a significant role for the surface modification of the target after irradiation either it is explored by SEM or AFM analysis. In order to explore small-scale structures (nanoscale) on the irradiated surface, too much refined surfaces of metal or alloys are required. Most real-life surfaces are not perfectly flat (not even near-perfect mirrors) and have certain degrees of texture and roughness to them, which will influence their optical behavior. Therefore, the polishing process can improve the surface texture by reducing the initial surface roughness. In our case the surface roughness of 10 nm is optimum, because we were only interested to explore micostructuring (ripples and craters) of laser-irradiated alloy.

On contrary, if the surface roughness is too high (say 50 nm) it will be difficult to explore craters and ripples with a scale height of less than 50 nm. Additionally, for higher initial surface roughness of 50 nm, the energy absorption of incoming electromagnetic radiation enhances significantly and consequently large-scale structures will be produced. Because for a laser-matter interaction and

processing application to be possible, the electromagnetic energy of the laser light needs to be transformed into thermal energy inside the metal. The amount of transformed energy is determined by the light absorption mechanisms in the metal. Absorption is also heavily dependent upon the surface properties of the metal or alloy. The initial surface roughness therefore influences significantly the optical behavior. Pits and valleys may, for instance, 'trap' some of the light and thereby enhance absorption.

The polished samples were annealed under a vacuum of 10^{-6} Torr by incorporating them in Pyrex glass tubes at a temperature of 300°C in a muffle furnace for 120 minutes. After mounting the samples on the sample holder, they were placed in the chamber, which was evacuated to the base pressure of 10^{-3} Torr.

An Excimer laser (KrF) of wavelength 248 nm, pulse duration of 18 ns, repetition rate of 30 Hz was employed to irradiate the sample under vacuum condition. The target samples were exposed for five various laser fluence of values 3.8, 4.3, 4.7, 5.1 and 5.5 J/cm^2 corresponding to the pulsed energies of 90, 100, 110, 120 and 130 mJ.

The incident laser beam, after passing through a Plano-convex lens of focal length 50 cm, was focused perpendicular to the target surface placed in the chamber. The whole experiment was performed at room temperature. All targets were treated with 2200 laser pulses. The samples were scanned with the help of a DC motor, thereby irradiating a scanned area of 235 mm × 1 mm. The surface morphology of the irradiated targets was investigated by a SEM (JEOL-JSM-6480LV).

In order to determine the crystallographic structure and phase analysis of the exposed targets an XRD X'Pert PRO multipurpose powder diffractometer was employed. The specimens were then subjected to deformation for hardness and tensile strength using a Vickers hardness tester (Zwick/Roell ZHU5030) and a universal tensile testing machine (AG-1 Shimadzu) to investigate microhardness and mechanical properties of Al–Cu alloy 2024.

3. Result and discussions

3.1. *Surface morphology*

Figure 1 shows the SEM images of (a) unirradiated and irradiated Al–Cu alloy 2024 for various laser fluences of (b) 3.8 J/cm^2, (c) 4.3 J/cm^2 (d) 4.7 J/cm^2 (e) 5.1 J/cm^2 and (f) 5.5 J/cm^2. For the fluence of 3.8 J/cm^2, a few micro-sized craters and ridges with non-uniform shape and density distribution are observed as shown in Figure 1(b).When the fluence is increased to 4.3 J/cm^2, the size, density and uniformity of craters increase as revealed in Figure 1(c). The appearance of multiple ablative layers and ripples is also seen at this fluence. Further increase in fluence to 4.7 J/cm^2 causes a decrease in the size of the craters as shown in Figure 1(d).The appearance of multiple ablative layers and ripples becomes more distinct at this fluence and significant changes in the density of the craters is observed.

When the fluence is increased up to 5.1 J/cm^2, the size of the craters decreases significantly and its uniformity and density increase as exhibited in Figure 1(e). Multiple ablative layers and ripples become more prominent at this fluence. Figure 1(f) depicts that at the maximum fluence of 5.5 J/cm^2, regular shaped craters are observed. The edges of these craters have been found to be uplifted. The crater formation as observed in Figure 1(b)–(d) can be attributed to thermal ablation on the basis of laser-induced heating, thermal desorption, melting and explosive boiling of the target surface (*6*, *7*). It has been investigated that if the surface temperature exceeds the melting and evaporation temperature of that material then fusion and evaporation take place. When the irradiation energy is higher than the ablation threshold, it leads to an ionization and results in plasma formation. The phenomena of melting and vaporization can be observed from the presence of molten materials around the craters (*8*). It has been also found that when the pressure of the

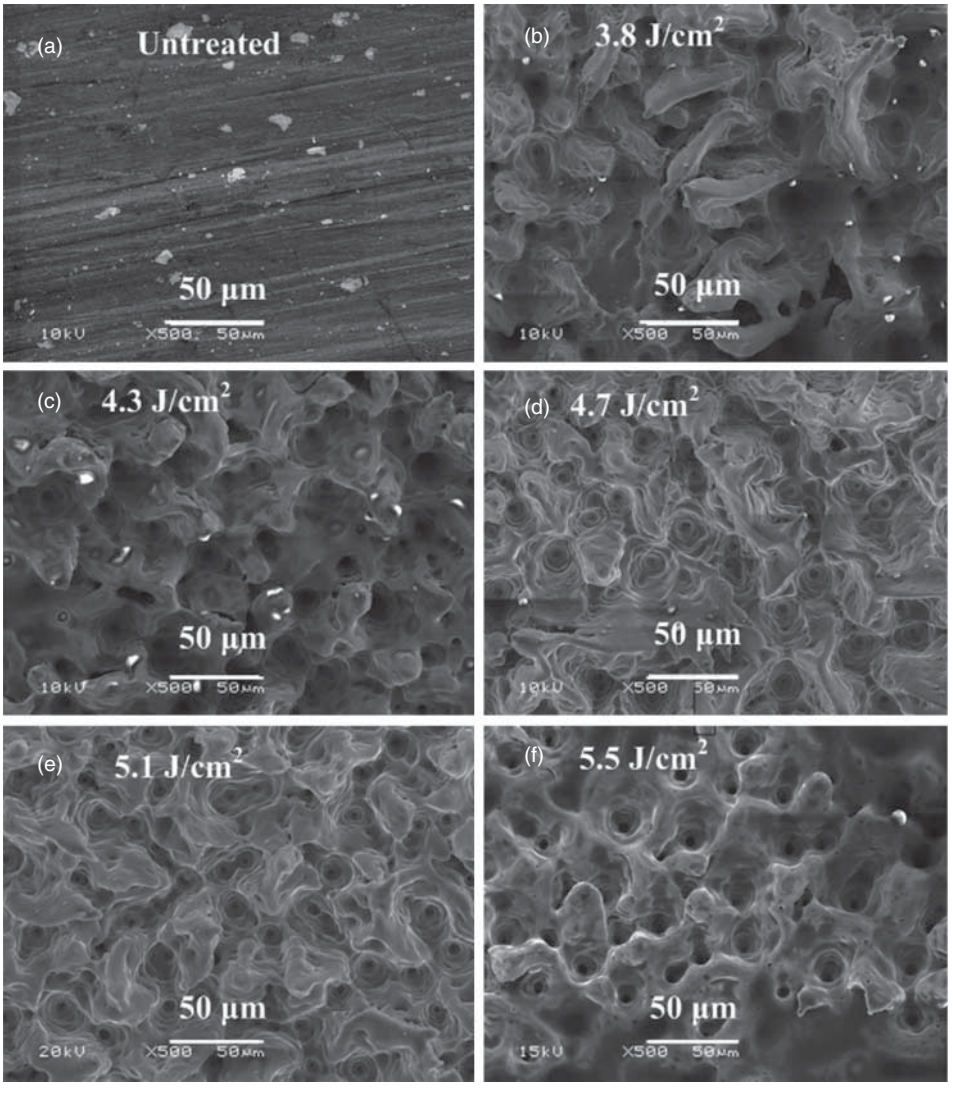

Figure 1. SEM micrographs revealing the comparison of variation in surface morphology of (a) unirradiated and irradiated Al-2024 alloy by 2200 pulses of Excimer laser at a wavelength of 248 nm, pulse duration of 18 ns and repetition rate of 30 Hz for various fluences of (b) 3.8 J/cm^2 (c) 4.3 J/cm^2 (d) 4.7 J/cm^2 (e) 5.1 J/cm^2 and (f) 5.5 J/cm^2.

plasma/vapor exceeds the surrounding pressure, the molten material can be expelled explosively from the target due to the violent recoil pressure. As a consequence, the crater is formed (*9*). The variations in the size of craters are attributed to a large number of surface defects such as inclusions, small pits, contaminants, oxides and other heterogeneities. These defects are generally associated with a higher sensitivity to laser absorption than the bulk material and hence cause the non-uniform laser energy absorption inside the material (*10*).

By increasing fluence from 3.8 to 4.3 J/cm^2 as shown in Figure 1(c), the increase in the crater size is attributed to the increase in recoil pressure with greater laser fluence. By increasing fluence upto 4.7 J/cm^2 as displayed in Figure 1(d), the crater size has been observed to be reduced which is primarily due to refilling of the melted material. With further increase in laser energy density up to the value 5.1 J/cm^2 as displayed in Figure 1(e), it has been observed that the crater size

decreases but the crater density does not increase, which can be explained by the accentuated local laser ablation effect due to more refilling of cavities. When the fluence is further increased up to a maximum value of 5.5 J/cm^2, the size of the craters becomes smaller due to intense melting, ablation, resolidification and refilling of the material as displayed in Figure 1(f) (*11*, *12*). Surface plasmons are produced due to coherent interaction of the incident laser field with free electrons created in the material. The formation of the ripples (periodicity) can thus be attributed to the excitation of the surface plasmons to induce the periodic enhancement of local fields in the surface layer. Thus, laser-material interaction is the reason for the development of compressive stresses which are responsible for the formation of defects and ripples in the interior of craters (*13*).

The fractographs of (a) unirradiated and irradiated Al–Cu alloy 2024 for various fluences of (b) 3.8 J/cm^2 (c) 4.3 J/cm^2 (d) 4.7 J/cm^2 (e) 5.1 J/cm^2 (f) 5.5 J/cm^2 are displayed in Figure 2. These fractographs reveal the appearance of micro-sized cavities. For an unirradiated sample, the density

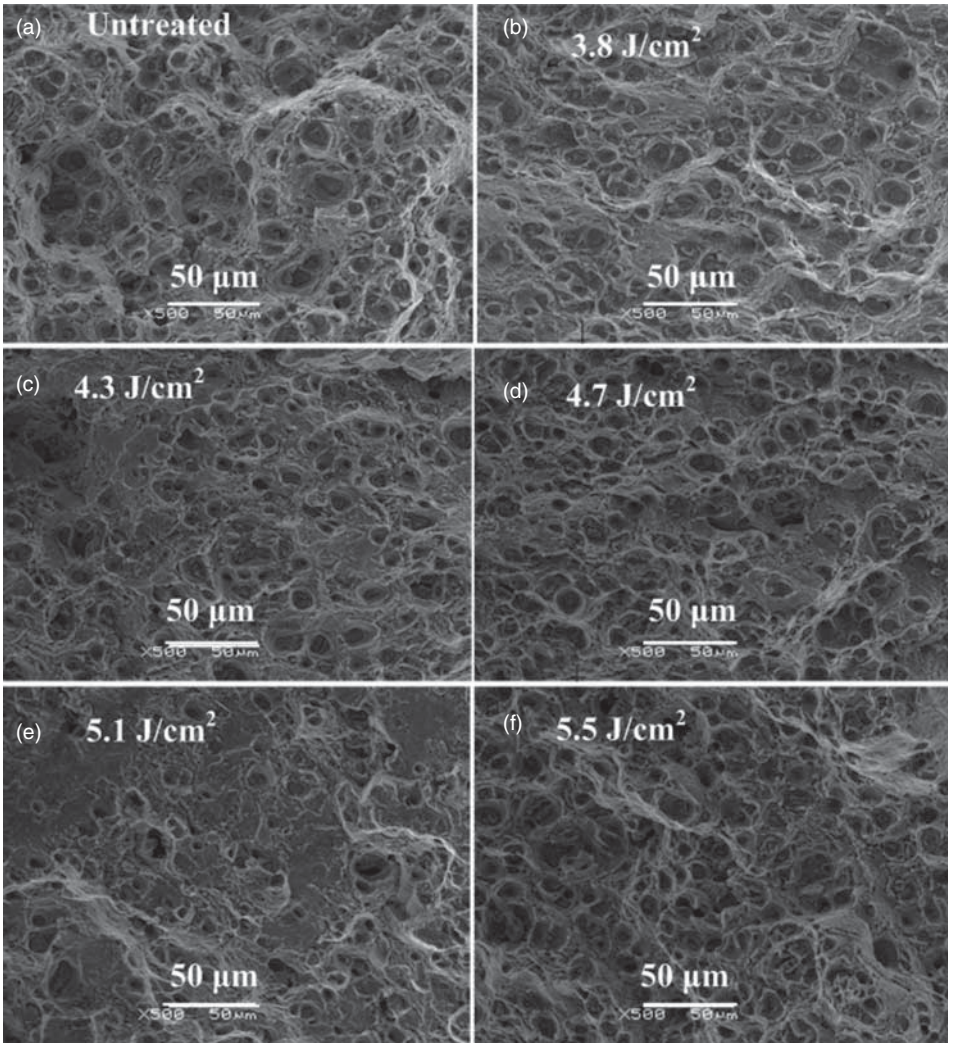

Figure 2. SEM fractographs revealing the comparison of variation in surface morphology of (a) unirradiated and irradiated Al-2024 alloy by 2200 pulses of Excimer laser at a wavelength of 248 nm, pulse duration of 18 ns and repetition rate of 30 Hz at different fluences of (b) 3.8 J/cm^2(c) 4.3 J/cm^2 (d) 4.7 J/cm^2 (e) 5.1 J/cm^2 and (f) 5.5 J/cm^2.

of cavities is small. The density of the cavities initially increases when the laser fluence increases from 3.8 J/cm^2 to a value of 4.3 J/cm^2. A decrease in the density of the cavities is observed when the fluence is further increased to its highest value of 5.5 J/cm^2 and at this fluence, cavities with maximum number density due to maximum heating, melting and consequently pronounced defect formation have been observed. The cracks are also seen in these fractographs. However, by increasing laser fluence, the density of the cracks increases and the surface shows large number of indentations as shown in the Figures 2(a)–(d). Hence, Figure 1 reveals the surface modification of alloy after irradiation and represents the appearance of craters at the surface, whereas fractographs of Figure 2 represent the generated defects in the form of cavities and cracks in bulk material after irradiation. However, in both figures the variation in the density and size of generated defects is anomalous.

3.2. *XRD analysis*

The XRD technique is used to obtain phase identification, variation in crystallinity, dislocation densities and energy deposited in the material. Figure 3 depicts the XRD patterns of (a) unirradiated and irradiated Al–Cu alloy 2024 under the vacuum condition for various laser fluences of (b) 3.8 J/cm^2 (c) 4.3 J/cm^2 (d) 4.7 J/cm^2 (e) 5.1 J/cm^2 and (f) 5.5 J/cm^2.

The diffraction peaks corresponding to (222), (213), (440) and (622) planes are observed for both unirradiated and irradiated specimen at angles 38°, 44°, 65° and 78°, respectively. Both the peak intensity and crystallinity of Al–Cu alloy 2024 specimen show an anomalous behavior for various fluences. The variations in the peak intensity are attributed to scattering effects, non-uniform

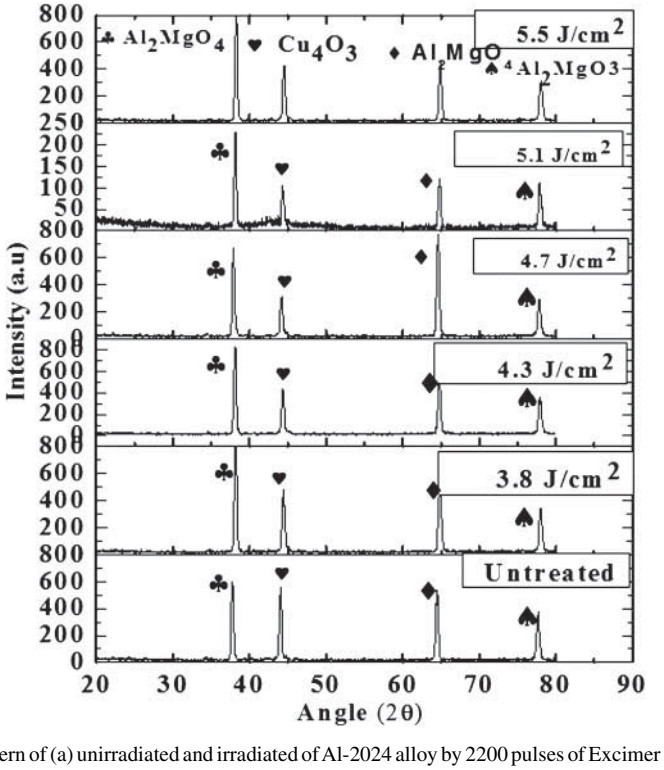

Figure 3. XRD pattern of (a) unirradiated and irradiated of Al-2024 alloy by 2200 pulses of Excimer laser at a wavelength of 248 nm, pulse duration of 18 ns and repetition rate of 30 Hz for various fluences of (b) 3.8 J/cm^2 (c) 4.3 J/cm^2(d) 4.7 J/cm^2 (e) 5.1 J/cm^2 and (f) 5.5 J/cm^2.

Table 1. Variation in the crystallite size of laser irradiated Al-2024 alloy for various fluences of 3.8 J/cm^2 (b) 4.3 J/cm^2 (c) 4.7 J/cm^2 (d) 5.1 J/cm^2 and (e) 5.5 J/cm^2.

Fluence (J/cm^2)	Crystallite size (nm)
3.8	35
4.0	50
4.7	20
5.1	47
5.5	56

thermal stresses, re-crystallization and non-uniform conduction of the energy absorbed by the atoms as a result of laser-matter interactions (*14*, *15*).

The crystallite size was evaluated using Scherer's formula (*16*)

$$\text{Crystallite size (D)} = \frac{0.9\lambda}{\beta \cos\theta}, \tag{1}$$

where 'λ' is wavelength of X-rays, 'β' is full wave half maxima and 'θ' is the angle of XRD. The variation of crystallite size with the fluence is represented in Table 1

The dislocation density has been evaluated by using following formula (*17*)

$$\text{Dislocation density} = \frac{1}{(\text{Crystallite size})^2}. \tag{2}$$

Initially, the peak intensity increases by increasing the fluence up to the value of 3.8 J/cm^2. This increase in peak intensity is attributed to the enhancement of diffraction of X-ray from target and the crystal growth caused by atomic diffusion across the grain boundaries after laser ablation. By increasing the fluence up to the value of 4.3 J/cm^2, the peak intensity decreases. Further increase in fluence up to the value of 4.7 J/cm^2 causes more reduction in peak intensity. The reason for the reduction of peak intensity is the re-crystallization phenomenon during resolidification. Large sized grains break up into the smaller ones after laser irradiation and cause the attenuation in the peak intensity.

Further increase in fluence up to a maximum value of 5.5 J/cm^2 causes enhancement of peak intensity which is related to the enhanced crystal growth due to maximum energy deposition. As the laser beam interacts with the material, the energy deposition initially generates defects. When energy deposition increases with increase in laser fluence, the defects are annealed. Further increase in laser fluence causes the generation of enhanced defects. Hence, the peak intensities initially increase and then decrease showing an anomalous behavior. Similarly, crystallite size and dislocation density initially increases then decreases and finally increases, hence reveals an anomalous behavior again. This variation in the crystallite size and dislocation density can be attributed to the thermal stresses, lattice defects and recovery processes (*18*, *19*).

The variation in the crystallite size and dislocation density for different laser fluences is shown in Figures 4 and 5.

Laser-induced pressure (GPa) and deposited energy (eV/atom) are also evaluated for various laser fluences and is plotted in Figure 6. With laser irradiation, different surface irregularities (protrusions and pits) emerge progressively with different geometrical sizes depending upon the laser fluence and the target selection. If the laser energy deposited (eV/atom) exceeds the heat of melting (threshold) per atom for a corresponding irradiated target, then localized and isolated defects can be observed at particular fluence. Therefore, it is important to calculate the deposited energy per atom for irradiated Al–Cu alloy 2024.

The deposited energy per atom is calculated using the following steps:

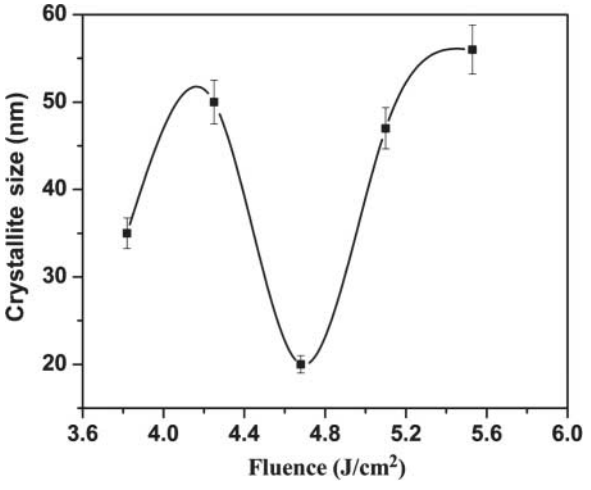

Figure 4. Variation in the crystallite size of laser-irradiated Al-2024 alloy for various fluences of (a) 3.8 J/cm^2 (b) 4.3 J/cm^2 (c) 4.7 J/cm^2 (d) 5.1 J/cm^2 and (e) 5.5 J/cm^2.

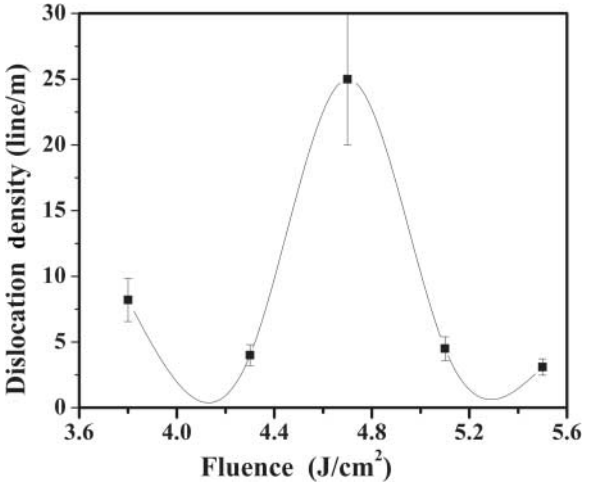

Figure 5. Variation of dislocation density of Al-2024 alloy irradiated for various fluences of (a) 3.8 J/cm^2 (b) 4.3 J/cm^2 (c) 4.7 J/cm^2 (d) 5.1 J/cm^2 and (e) 5.5 J/cm^2.

Energy per pulse E (J) can be converted into energy in eV/nm^2, *i.e.*

Area of the rectangular focused laser spot $= a \times b$,

where 'a' is the length and 'b' is the width of the rectangular beam.

The length and width of rectangular beam are measured by irradiating the target material with laser radiation and then exploring the surface by using SEM analysis.

Here $a = 0.235$ cm and $b = 0.1$ cm for the Excimer laser.

Therefore, the area of the rectangular focused laser spot $= 0.0235\,\text{cm}^2$

Using 1 eV $= 1.6 \times 10^{-19}$ J

$$\text{Energy}(\text{eV/m}^2) = \frac{E \times 10^{-3}}{1.6 \times 10^{-19}} \left\{ \frac{10,000 \times 10,000}{0.235 \times 0.1} \right\} = E \times 26.60 \times 10^{24}\ \text{eV/m}^2.$$

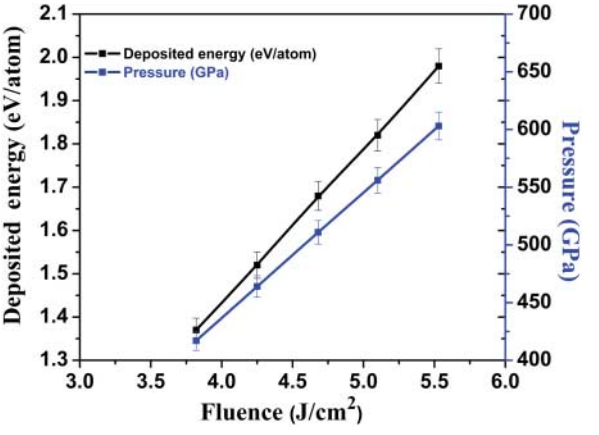

Figure 6. Variation of deposited energy (eV/atom) and pressure (GPa) of laser-irradiated Al-2024 alloy for various fluences of (a) 3.8 J/cm^2 (b) 4.3 J/cm^2 (c) 4.7 J/cm^2 (d) 5.1 J/cm^2 and (e) 5.5 J/cm^2.

Now the energy deposited per unit volume (eV/m^3) in a skin layer (l_s) excited by ns-laser is defined by the following relation:

$$E_{\text{abs}} \cong E\frac{(\text{eV/m}^2)}{l_s}. \tag{3}$$

A laser beam with 248 nm wavelength excites Al–Cu alloy 2024 in the skin layer $l_s = 8.7$ nm.

The optical properties of the material (reflection or absorption at 248 nm) affect the energy deposition of the specific material. An absorption coefficient $A = (1 - R) = 1 - 0.90526 = 0.09474$ (where R is surface reflectivity and A is absorption) at 248 nm for Al–Cu alloy 2024.

The real value of energy deposited (eV/m^3) is calculated by multiplying Equation (1) with an absorption coefficient of the corresponding material as (*20*)

$$\begin{aligned} E_{\text{abs}} &\cong AE\ (\text{eV/m}^3), \\ E_{\text{abs}} &= E \times 3.05 \times 10^{33}\ (\text{eV/m}^3), \end{aligned} \tag{4}$$

where values of energy range has been taken to be 90, 100, 110, 120, 130 J. In order to calculate the energy deposited per atom (eV/atom), the number of atoms per unit volume (atom/nm^3) must be known. The number of atoms per cm^3 is known to be 1.9×10^{24} for Al–Cu alloy 2024. The number of atoms per m^3 is 190×10^{28}. By dividing energy deposited per unit volume (eV/m^3) by the number of atoms (190×10^{28} atoms/m^3), energy deposited per atom has been calculated.

It is observed that both pressure and deposited energy per atom increase with increasing laser fluence. The increase in pressure and deposited energy with the increase in laser fluence can be attributed to compression stresses and deposition of energy during laser interaction. Our results also conform to this finding (*21*).

3.3. *Tensile testing*

The stress–strain curves of (a) unirradiated and irradiated Al–Cu alloy 2024 alloy for various fluences of (b) 3.8 J/cm^2 (c) 4.3 J/cm^2 (d) 4.7 J/cm^2 (e) 5.1 J/cm^2 (f) 5.5 J/cm^2 are exhibited in Figure 7.

The variations of the YS, UTS and percentage elongation evaluated from the tensile curves for various laser fluences are plotted in Figures 8 and 9. The YS and UTS of the specimen initially

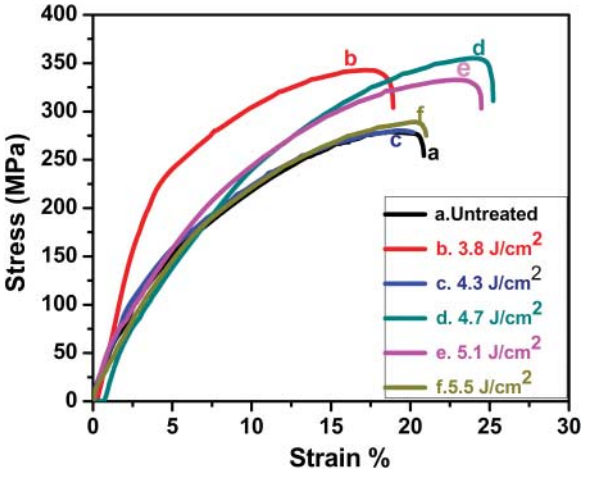

Figure 7. The stress–strain curves of unirradiated and laser-irradiated Al-2024 alloy for various fluences of (a) 3.8 J/cm^2 (b) 4.3 J/cm^2 (c) 4.7 J/cm^2 (d) 5.1 J/cm^2 and (e) 5.5 J/cm^2.

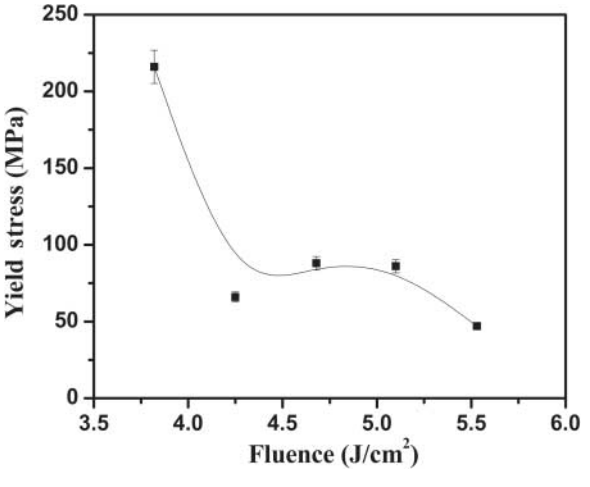

Figure 8. Variation of yield stress of irradiated Al-2024 alloy for various fluences of (a) 3.8 J/cm^2 (b) 4.3 J/cm^2 (c) 4.7 J/cm^2 (d) 5.1 J/cm^2 and (e) 5.5 J/cm^2.

increase after laser irradiation at a fluence of 3.8 J/cm^2. However, a decrease in both is observed when the fluence is increased to the value of 4.3 J/cm^2. Again an increasing trend in both YS and UTS is observed for a higher fluence of 4.7 J/cm^2. Afterward, a monotonic decrease is observed with further increase in fluence from 5.1 to 5.5 J/cm^2, respectively.

Similarly, the percentage elongation of the specimen after irradiation decreases at a fluence of 3.8 J/cm^2 and then increases at 4.3 J/cm^2. With increase in the fluence from 4.7 to 5.5 J/cm^2, a monotonic decrease in percentage elongation is observed. These variations in the value of 'YS' and 'UTS' may be attributed to the changes in microstructure and dislocation density as the laser-material interaction takes place.

When laser fluence is increased up to the value of 3.8 J/cm^2, it generates enough heat due to which the density of the defects increases and enhanced stresses are produced due to shock waves which causes increased tensile strength of the material (*22*). The improvements of hardness and elastic modulus of exposed targets in comparison with unexposed target are correlated with the

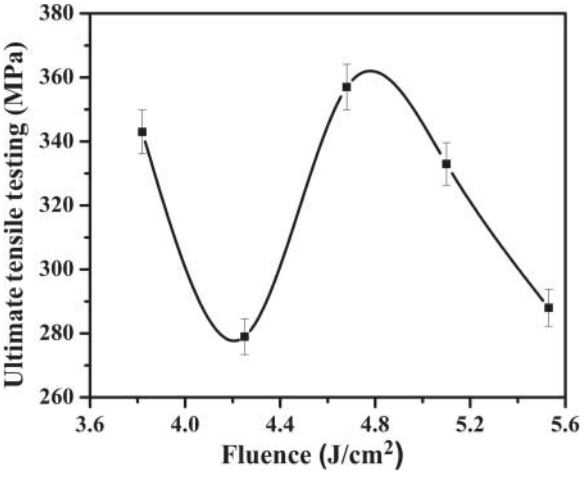

Figure 9. Variation of UTS of irradiated Al-2024 alloy for various fluences of (a) 3.8 J/cm^2 (b) 4.3 J/cm^2 (c) 4.7 J/cm^2 (d) 5.1 J/cm^2 and (e) 5.5 J/cm^2.

generation of the dislocation density, grain size and the microstructural deformation (*23*, *24*). A reduced density of defects causes a decrease in the tensile strength (*23*, *25*). When the fluence is increased to 4.3 J/cm^2, crystallite size increases and dislocation density decreases due to which 'YS' and 'UTS' decrease. We assume that a more pronounced material heating and cooling have taken place which causes annealing of the material and thus is responsible for the reduction of defect density When the fluence is increased to the value of 4.7 J/cm^2, the crystallite size decreases and dislocation density increases which also induce a high level of residual stress in the specimen, as a result, 'YS' and 'UTS' increase. This increase may also be due to the generation of more defects with the increase in laser fluence. When fluence is further increased from 4.7 J/cm^2 to its maximum value of 5.5 J/cm^2, the crystallite size increases and dislocation density decreases due to merging of defects and resolidification of the material and hence as a result, decreases in the value of 'YS' and 'UTS' of the material have been observed.

Hence, we conclude that the tensile properties of Al–Cu alloy 2024 show an anomalous behavior mainly due to grain refinement, generation of density dislocations and variation in the density of defects with increasing laser fluence. Such sort of anomalous behavior of 'YS' and 'UTS' has not been observed first time. Such behavior was also observed by other research groups. For example, Khaliq et al. (*26*) reported that Ti alloy shows anomalous behavior when it is irradiated with laser.

3.4. *Microhardness*

Figure 10 shows variation in the value of the microhardness from 88 to 116 HV for different fluences of values from 3.8 to 5.5 J/cm^2. The microhardness initially decreases by increasing fluence from 3.8 to 4.3 J/cm^2. When the fluence is increased from 4.3 to 5.1 J/cm^2, an increase in the microhardness is observed. Further increase in the fluence up to 5.5 J/cm^2 causes reduction in the microhardness of the irradiated material. The changes in microhardness are attributed to the lattice disorder, associated with changes in crystal structure and thermal compressive stresses produced in the material as a result of laser-induced heating (*18*, *19*). The change in microhardness can also be correlated with the change in dislocation density and crystal size as has been evaluated by XRD analysis and is shown in Figures 4 and 5. By decreasing the grain size and increasing the dislocation density, microhardness increases (*22*).

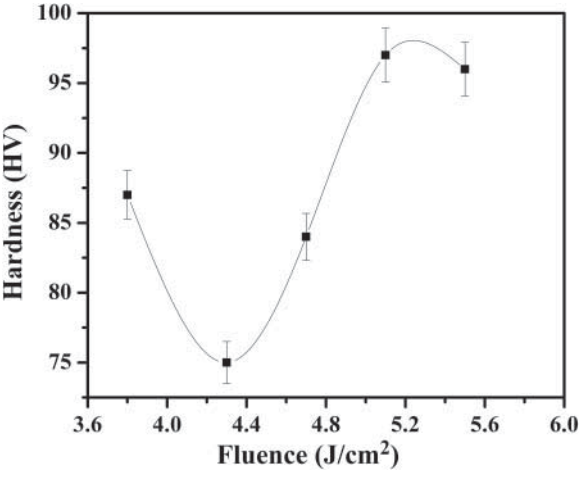

Figure 10. Variation of the microhardness of irradiated Al-2024 alloy for various fluences of (a) 3.8 J/cm^2 (b) 4.3 J/cm^2(c) 4.7 J/cm^2 (d) 5.1 J/cm^2 and (e) 5.5 J/cm^2.

4. Conclusions

The laser irradiation effects on the surface, structural and mechanical modification of Al–Cu alloy 2024 has been revealed. SEM results reveal the appearance of crater formation along with laser-induced periodic surface structures and multiple ablative layers. By increasing laser fluence, the size of the craters initially increases and then decreases. From XRD results, it is observed that peak intensity, crystalline size and dislocation density of the irradiated target exhibit anomalous behavior by increasing laser fluence. The tensile testing results reveal the dependence of YS, UTS and elongation upon the laser fluence. Similarly, the microhardness also shows anomalous behavior for various laser fluences. The observed changes in the mechanical properties are well correlated with surface and structural modification of irradiated sample.

References

(1) Parkhill, R.L.; Knobbe, E.T. *Proc. SPIE*. **1997,** *2992,* 81–85.
(2) Peercy, P.; Draper, C.; Mazzoldi, P. *Laser Surf. Treatment Metals*. **1986,** *115,* 57–78.
(3) Dou, K.; Knobbe, E.T.; Parkhill, R.L.; Wang, Y. *IEEE. J. Quant. Electro*. **2000,** *6,* 689–695.
(4) Hong, Z.; Chengye, Y. *Mat. Sci. Eng. A*. **1998,** *257,* 322–327.
(5) Yang, J.M.; Her, Y.C.; Han, N.; Clauer, A. *Mat. Sci. Eng. A*. **2001,** *298,* 296–299.
(6) Chrisey, D.B.; Hubler, G.K. *Pulsed Laser Deposition*; John Willey & Sons: New York, 1994.
(7) Perez, D.; Lewis, L. *J. Phys. Rev. Lett*. **2002,** *89,* 255504–255508.
(8) Chichkov, B.N.; Momma, C.; Nolte, S.; Alvensleben, F.V.; Tünnermann, A. *J. Appl. Phys. A*. **1996,** *63,* 109–115.
(9) Koner, C.; Mayerhofer, R.; Hartmann, V.; Bergmann, H.W. *J. Appl. Phys. A*. **1996,** *63,* 123–131.
(10) Dauscher, A.; Feregotto, V.; Cordier, P.; Thomy, A. *Appl. Surf. Sci*. **1996,** *410,* 96–98.
(11) Fairand, B.P.; Clauer, A.H.; Wilcox, B.A. *Metal Transac. A*. **1977,** *8,* 1871–1877.
(12) Gerland, M.; Hallouin, M.J. *Mat. Sci.* **1994,** *29,* 345–351.
(13) Huang, M.; Zhao, F.; Cheng, Y.; Xu, N.; Xu, Z.Z. *ACS Nano*. **2009,** *3,* 4062–4070.
(14) Chand, M. *Science of Engineering Materials: Structure of Matter*, Macmillan: London, 1981.
(15) Cullity, B.D. *Elements of X-Rays Diffraction*; Addison-Wesley: Boston, 1978.
(16) Cullity, B.D.; Stock, S.R. *Elements of X-Ray Diffraction*, 3rd ed.; Prentice-Hall: Upper Saddle River, NJ, 2001.
(17) Venkatachalam, S.; Rajendra, K.R.T.; Mangalaraj, D.; Narayandass, S.K.; Kim, K.; Junsin, Y. *Sol. Elect*. **2004,** *48,* 2219–2223.
(18) Hull, D.; Bacon, D. *Introduction to Dislocations*; Butterworth-Heinemann: Jordon Hill, Oxford, 2001.
(19) Smith, W.F. *Principles of Material Sciences and Engineering*, 2nd ed.; McGraw Hill: Tokyo, 1990.
(20) Allen, M.V. *Laser Beam Interaction with Materials*; Springer: Berlin, 1987.

(21) Juodkazis, S.; Nishimura, K.; Tanaka, S.; Misawa, H.; Gamaly, E.G.; Luther, D.B.; Hallo, L.; Nicolai, P.; Tikhonchuk, V.T. *Phys. Rev. Lett*. **2006,** *96,* 166101–166104.
(22) Fournier, J. Modern Mechanical Surface Treatment. Dissertation, Ecole Polytechnique, Paris, 1989.
(23) Peyre, P.; Fabbro, R.; Merrien, P.; Lieurade, H.P. *Mater. Sci. Eng. A*. **1996,** *210,* 102–113.
(24) Yilbas, B.S.; Arif, A.F.M. *J. Phys. D: Appl. Phys*. **2007,** *40,* 6740–6747.
(25) Fourier, J. *Mater. Manufac. Process*. **1990,** *5,* 144–151.
(26) Khaliq, M.; Farid, N.; Ghauri, I.M.; Afzal, N.; Adrees, Y.; Mubarik, F.E. *Phys. Scrip*. **2010**, *82,* 045606–045612.